

Scale-Aware Relay and Scale-Adaptive Loss for Tiny Object Detection in Aerial Images

Jinfu Li^{ID}, Yuqi Huang^{ID}, Hong Song^{ID}, Ting Wang^{ID}, Jiangnan Xia^{ID}, Yucong Lin^{ID}, Jingfan Fan^{ID}, Jian Yang^{ID}

Abstract—Recently, despite the remarkable advancements in object detection, modern detectors still struggle to detect tiny objects in aerial images. One key reason is that tiny objects carry limited features that are inevitably degraded or lost during long-distance network propagation. Another is that smaller objects receive disproportionately greater regression penalties than larger ones during training. To tackle these issues, we propose a Scale-Aware Relay Layer (SARL) and a Scale-Adaptive Loss (SAL) for tiny object detection, both of which are seamlessly compatible with the top-performing frameworks. Specifically, SARL employs a cross-scale spatial-channel attention to progressively enrich the meaningful features of each layer and strengthen the cross-layer feature sharing. SAL reshapes the vanilla IoU-based losses so as to dynamically assign lower weights to larger objects. This loss is able to focus training on tiny objects while reducing the influence on large objects. Extensive experiments are conducted on three benchmarks (*i.e.*, AI-TOD, DOTA-v2.0 and VisDrone2019), and the results demonstrate that the proposed method boosts the generalization ability by 5.5% Average Precision (AP) when embedded in YOLOv5 (anchor-based) and YOLOx (anchor-free) baselines. Moreover, it also promotes the robust performance with 29.0% AP on the real-world noisy dataset (*i.e.*, AI-TOD-v2.0).

Index Terms—Tiny object detection, discriminative features, scale-aware attention network, scale-adaptive loss.

I. INTRODUCTION

TINY object detection (TOD) is always a fundamental task in aerial image processing, aiming to categorize and locate highly structured objects with fewer than 16×16 pixels, such as persons, ships and vehicles. These tiny objects appear everywhere in practical applications, where their accurate detection is beneficial to automated interpretation and informed decision-making [1]–[4]. However, the shooting angle and imaging altitude enable the size, shape, and orientation of objects to vary so much that extracting sufficient appearance information is extremely difficult [5]. Meanwhile, changes in light and weather further complicate the backgrounds, leading to a low signal-to-noise ratio (SNR) [6]. The cumulative effects of these factors pose significant challenges for TOD, making it a hotspot in both academia and industry circles.

With the rapid development of deep neural networks [7]–[9], generic object detection has made great progress. Many studies

This work was supported in part by the National Natural Science Foundation of China (No. 62025104, 62171039 and U22A2052) and in part by the Natural Science Foundation of Beijing, China (No. L242024). (Corresponding authors: Hong Song and Jian Yang; E-mail: songhong@bit.edu.cn and jyang@bit.edu.cn.)

Jinfu Li, Yuqi Huang, Hong Song, Ting Wang and Jiangnan Xia are with the School of Computer Science and Technology, Beijing Institute of Technology, Beijing 100081, China.

Yucong Lin, Jingfan Fan and Jian Yang are with the School of Optics and Photonics, Beijing Institute of Technology, Beijing 100081, China.

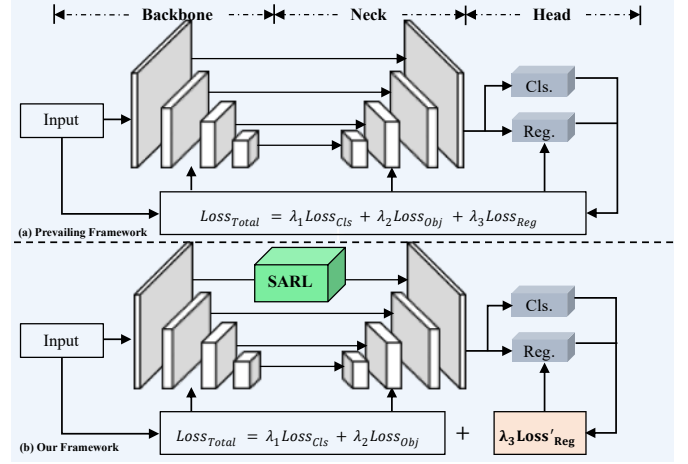


Fig. 1. Schematic illustration of the comparison between the prevailing framework and our framework. (a) Prevailing Framework. (b) Our Framework.

suggested that general detectors, even the most advanced ones, will not produce satisfactory results if directly applied to the TOD task [10]. The alternatives usually assemble some special design and/or mechanisms into the top of general detectors. A common strategy is to increase the number of tiny objects in the dataset, thereby enhancing the model's ability to learn their representations. These data augmentation techniques include Generative adversarial networks (GAN)-based object synthesis [11], image pyramid [12], aggregated-mosaic [13], copy-paste [14], and so on. However, these methods entail a compromise in computational costs. Given the scarcity of visual cues, it is necessary to mine and exploit extra semantic and contextual information. For instance, Cheng *et al.* [15] employed cross-attention and self-attention network (RCSANet) to match key points with regional backgrounds. Chen *et al.* [16] utilized multiple kernel dilated convolution to expand the receptive field without reducing the spatial resolution. Moreover, a lot of efforts have been made on bottom-up and top-down structures [17]–[19]. Recently, researchers began exploring new similarity metrics to replace IoU in NMS (Non-Maximum Suppression), loss functions, and label assignment [20]–[23]. In [20], the Sig-NMS is proposed to adjust the threshold by a fraction reset function, which mitigates the problem of tiny objects being suppressed in original NMS. Xu *et al.* [21] projected high-dimensional features into 2D Gaussian distributions and adopted the normalized Wasserstein distance (NWD) to represent the location relationship. Later, Xu *et al.* [22] also proposed a receptive field-based label assignment (RFLA) strategy, which took a Gaussian receptive field distance to

calculate the similarity between predictions and ground truths. While the preceding methods have shown promise, there is still plenty of room for improvement on two issues.

(i) *Discriminative features degrade or get lost as they propagate through the detection network.* Current mainstream detectors typically consist of three key parts: the backbone, neck, and head. The backbone mainly employs a cascade of convolutional and pooling layers to generate hierarchical feature maps. As the layers deepen, these maps increasingly contain semantic information, which helps recognize objects with diverse scales and contexts. However, this downsampling procedure inevitably reduces the spatial resolution and discards spatial details that are crucial for distinguishing tiny objects from their backgrounds and from one another. Additionally, the neck (e.g., FPN [24], PANet [25], and BiFPN [26]) directly utilizes a series of operations like upsampling, concatenation, and skip/lateral connections to aggregate low-layer and high-layer feature maps. Ideally, it should work in harmony with the backbone, with each part leveraging its unique strengths to build a comprehensive feature pyramid. However, the neck largely relies on the quality and completeness of the input to be effective. Weak or incomplete feature maps prevent the neck from refining them, causing a cascading effect that exacerbates the performance of the entire detection network.

(ii) *Unfair regression penalties are imposed on tiny objects in bounding box predictions.* As we all know, IoU is the most familiar metric for evaluating the accuracy of predictions. The regression losses based on IoU and its derivatives (e.g., GIoU [27], DIoU and CIoU [28]) have been proven effective in guiding the model to learn precise bounding box coordinates. Nevertheless, when these losses are implemented in TOD, a significant disparity in penalty arises. Concretely, large objects, due to larger pixels areas, exhibit a higher tolerance for deviations in localization without sharp drops in IoU values. This means that the model prioritizes optimizing its performance on large objects since they contribute less to the regression loss. In contrast, tiny objects have a greater sensitivity to localization deviations. Even minor positional shifts can decay IoU values rapidly. As a result, these values translate into disproportionate penalties in the calculation of the regression loss, focusing the model less on tiny objects.

To mitigate the above issues, this paper introduces a Scale-Aware Relay Layer (SARL) and a Scale-Aware Loss (SAL) for tiny object detection. Both can be smoothly integrated into previous methods. SARL incorporates a cross-scale spatial-channel attention mechanism that refines and enhances the hierarchical feature maps extracted by the backbone before feeding them into the neck. This mechanism exploits high-level semantic information to reweight low-level spatial information from adjacent layers. By doing so, SARL preserves and amplifies the fine-grained details that are often weakened or lost during network traversal while suppressing redundant information. Additionally, SAL is a dynamically scaled IoU-based regression loss, where the scaling factor decreases fast as the object's area increases. In fact, this scaling factor automatically reduces the penalty of larger objects during training, enabling the model focus more on tiny objects. To validate SARL and SAL, we conducted extensive experiments on four public

datasets and compared their performance when integrated with anchor-based (YOLOv5) and anchor-free (YOLOx) object detection frameworks. Our results demonstrate the effectiveness of this approach in improving the overall performance, particularly in challenging noise scenarios.

The main contributions are summarized as follows:

- We design the scale-aware relay layer (SARL), positioned between the backbone and neck, to selectively emphasize the regions of interest while suppressing irrelevant features, thereby preventing the loss of fine-grained details.
- We design the scale-adaptive loss (SAL), which dynamically assigns regression penalties to objects based on their scale, ensuring a robust training against scale variations.
- We incorporate SARL and SAL into the popular anchor-based YOLOv5 and anchor-free YOLOx object detection algorithms, respectively, and demonstrate their performance improvement on four major benchmarks.

The rest of this paper is organized as follows. In Section II, we provide a brief overview of related work in object detection and tiny object detection. In Section III, we describe the architecture and design of the SARL and SAL in detail. In Section IV, we present our experimental setup and results, including a comparison with state-of-the-art detection models. Finally, in Section V, we conclude our findings and discuss potential future directions for research in this area.

II. RELATED WORK

A. Generic Object Detection

Object detection methods can be roughly grouped into anchor-based and anchor-free detectors, depending on whether the pre-defined anchor boxes are used. The former utilizes one-stage or two-stage networks to generate region proposals and perform classification. Instead, the latter directly predicts the bounding boxes by keypoint-based or center-based networks.

1) *Anchor-based Detectors:* One-stage networks, such as SSD [29], RetinaNet [30], and YOLO family [31]–[33], prioritized speed and real-time performance. They accomplished this by classifying and regressing bounding boxes in a single pass through the network, making them ideal for applications where latency is a critical factor. In contrast, two-stage networks, exemplified by FPN [24], R-CNN family [7], [8], [34], [35], and TridentNet [36], emphasized higher accuracy by first creating a set of region proposals and then refining these proposals through a second stage of classification and bounding box regression. This two-step process allowed for more precise localization and classification of objects, making two-stage networks effective in scenarios requiring high accuracy.

2) *Anchor-free Detectors:* Keypoint-based networks inferred bounding boxes from the geometrical relationships of multiple key points. CornerNet [37] detected the top-left and bottom-right corners with embedding vectors, while CenterNet [38] added the center point into the detection. Other representative works included Grid R-CNN [39], RepPoints [40], and FoveaBox [41]. In contrast, center-based networks mainly identified the center point. FCOS [42] computed distances from the center to the box boundaries, and TOOD [43] optimized anchor points via a task alignment learning strategy.

Meanwhile, FCOS and TOOD have also introduced into the YOLO series, e.g., YOLOx [44] and YOLOv8 [45]. Obviously, anchor-free detectors offered a compelling alternative, especially in resource-limited or highly variable detection tasks.

B. Tiny Object Detection

1) *Discriminative Feature Learning*: It is well-known that tiny objects have limited appearance information. Researchers have therefore investigated various methods to improve the learning of discriminative features for them. In [18], Li *et al.* proposed a cross-layer attention mechanism after down-sampling and upsampling procedures to strengthen the expression of spatial and context information. In [19], [46], the authors tried to establish the connection between different level features and combine them by a bidirectional FPN. Wu *et al.* [47] introduced a feature-and-spatial aligned network (FSANet) where a novel feature-aware alignment module is designed to align adjacent features of different resolutions, facilitating the extraction of more discriminative features. Like RCSANet [15], FSANet also followed an anchor-free paradigm that could reduce the position-sensitive influences on tiny objects. Besides, several early mentioned works [16], [17] on hierarchical feature learning and interaction have shown impressive performance. However, these methods preferred to design suitable network structures to enrich discriminative features, overlooking the coordination with the training strategies.

2) *Improved Detection Metrics*: As stated in Section I, several excellent studies (e.g., NWD [21] and RFLA [22]) have highlighted the challenges associated with most IoU-based detection metrics in handling position deviation and delineating object boundaries. Thus, there is a trend towards creating specialized metrics for NMS, loss functions, and label assignment processes [48]–[50]. In their research, Xu *et al.* [48] introduced the Dot Distance (DotD), which is defined as the normalized Euclidean distance between the center points of two bounding boxes. Zhou *et al.* [49] proposed the use of the Kullback-Leibler divergence (KLD) as a replacement for the NWD [21] to select more positive instances of tiny objects. In [50], Su *et al.* firstly modelled bounding boxes as 2D Gaussian distributions similar to [21] and [49]. They then designed a new metric called Mixed Minimum Point-Wasserstein (MMPW) to analyze these Gaussian distributions rather than NWD and KLD. However, the preceding methods mainly concentrated on optimizing training strategies, while lacking in-depth exploration of discriminative features.

In summary, both approaches have their respective focuses yet fall short in achieving optimal accuracy and generalization. Therefore, this paper proposes the Scale-Aware Relay Layer (SARL) and Scale-Adaptive Loss (SAL) to merge their merits and enhance model performance. SARL dynamically adjusts information flow within the network based on input feature scale, ensuring effective propagation of relevant features through a cross-layer attention mechanism that considers both semantic and spatial information. Additionally, SAL complements SARL by modulating error penalties based on object scale, enabling the model to pay more attention on smaller objects while maintaining robustness for larger ones.

III. PROPOSED METHOD

In this section, we describe our method in detail. First, Section III-A introduces the overview of the proposed framework. Then, Section III-B presents the Scale-Aware Attention Network (SA^2N). Finally, the Scale-Feedback Loss (SFL) is introduced in Section III-C.

A. Overall Framework

Before discussing the particular architecture as shown in 2, we should clarify the main design ideal first. The current object detection paradigms faces two main challenges in effectively identifying small objects in aerial images, namely the degradation of discriminative features during feature aggregation and the significant imbalance in regression loss of objects of different scales. To this end, we propose a novel approach that combines mix-attention mechanism with scale-aware optimization strategy to improve the quality of discriminative features and balance the regression loss across various scales.

1 shows a comparison between our framework and prevailing frameworks. From 2, it can be seen that SA^2N is one of our main innovations. This work aims to address a critical bottleneck: the insufficiency or loss of discriminative features during pyramid feature aggregation processes. Existing feature extraction paradigms often fail to provide adequate multi-level discriminative features, which is crucial for accurate tiny object detection. This problem is exacerbated by the down-sampling and pooling processes in the network's backbone, resulting in blurred appearances of the targets and their low signal-to-noise ratios. To mitigate these issues, our approach introduces the Self-Attention Aggregated Network (SA^2N). SA^2N leverages attention mechanisms to adaptively weight the pyramidal feature hierarchy extracted from the backbone. By doing so, it enhances the quality of multi-scale features, facilitating effective bidirectional aggregation and significantly improving the network's capability to detect small objects in complex aerial imagery environments.

Moreover, as shown in 2, our method incorporates the Scale-Feedback Loss (SFL), which uses scale-feedback signals to calculate localization errors, thereby promoting balanced network training. The SFL mechanism ensures that the regression loss is distributed evenly across various scales, which is crucial for achieving consistent detection performance. This balance addresses another critical issue in tiny object detection, where different scales can lead to inconsistent loss contributions.

Both SA^2N and SFL are designed to be compatible with a wide range of detection frameworks, including both anchor-based and anchor-free detectors that utilize IoU-based regression loss. This compatibility provides flexibility and robustness, making our approach versatile for different application scenarios. SA^2N 's ability to extract precise dense features is pivotal in improving detection accuracy, particularly for small objects. The combination of a mix-attention mechanism with a scale-aware optimization strategy in our novel approach significantly advances object detection technologies. It ensures that even in the presence of complex aerial imagery, tiny objects can be detected with high precision and reliability.

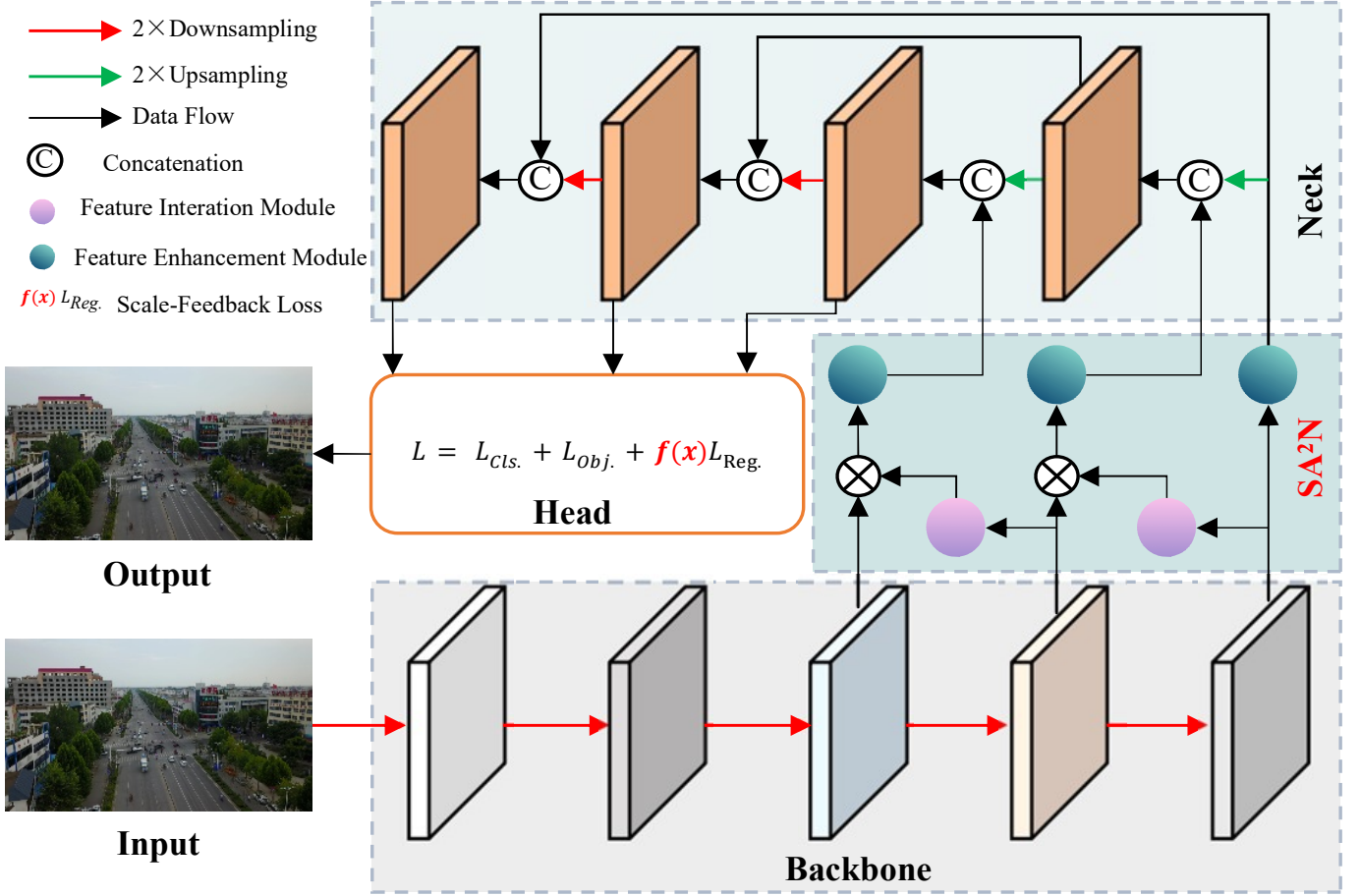


Fig. 2. Overall framework of our method. SA^2N is used to enhance discriminative features. SFL is used to balance the regression loss.

B. Scale-Aware Attention Block

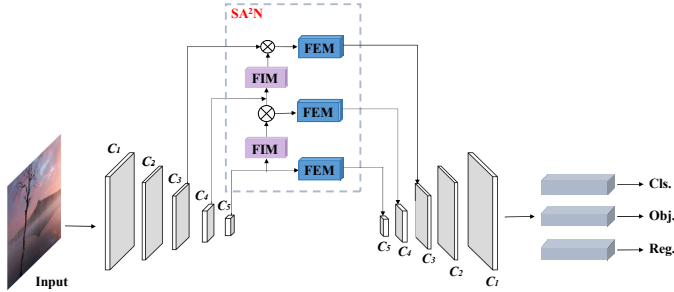


Fig. 3. Position and overall structure of SA^2N .

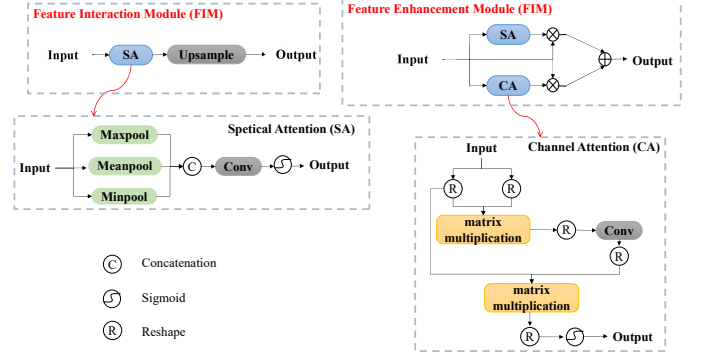


Fig. 4. Specific structure of FIM and FEM .

C. Scale-Feedback Loss

In common with other object detection methods, the loss function of our framework takes the form of multi-task loss, which is defined as

$$Loss = Loss_{cls} + Loss_{obj} + Loss_{pos} \quad (1)$$

where $Loss_{cls}$, $Loss_{obj}$, and $Loss_{pos}$ represent classification loss, confidence loss, and positional loss, respectively. Both

$Loss_{cls}$ and $Loss_{obj}$ use the cross-entropy loss (CE). It can be formulated in the following form.

$$Loss_{cen} = -\frac{1}{N} \sum_{i=1}^n [a_i \log \sigma(a'_i) + (1-a_i) \log (1-\sigma(a'_i))] \quad (2)$$

where $Loss_{cen}$ denotes the CE loss. a'_i represents the predicted value of the model: for classification loss, it is the predicted classification score of prediction box i , and for confidence loss, it is the predicted confidence score of the model on the likelihood of the object in the corresponding grid of prediction

box i . a_i represents the true label: for classification loss, it is the true category label of the object, and for confidence loss, it is the true score of whether the object exists in the corresponding grid of prediction box i .

In order to alleviate the imbalance of regression loss, we use SFL to replace the original IoU Loss as part of the position loss. The position loss of our model is as follows (The position loss is a combination of SFL and L1 loss, it can be formulated in the following form.):

$$Loss_{pos} = Loss_{l1} + \alpha Loss_{SFL} \quad (3)$$

where α is a regulatory factor used to regulate the ratio of L1 loss and SFL . L1 loss can be formulated in the following form.

$$Loss_{l1} = \frac{\sum_{i=1}^n |a'_i - a_i|}{n} \quad (4)$$

$$(a_i = x_i, y_i, h_i, w_i; a'_i = x'_i, y'_i, h'_i, w'_i)$$

where x_i, y_i, h_i, w_i respectively represent the top left horizontal and vertical coordinates, width and height of the ground truth i , and x'_i, y'_i, h'_i, w'_i respectively represent the top left horizontal and vertical coordinates, width and height of the predicted box i . a_i and a'_i are respectively substituted with x_i, y_i, h_i, w_i and x'_i, y'_i, h'_i, w'_i , and the L1 loss of the horizontal and vertical coordinates, width, and height of the top left corner of the prediction box i can be calculated.

SFL can be formulated in the following form.

$$Loss_{SFL} = \sum_{i=1}^n \beta \ln(2 - s_i)(1 - IoU_i^2)$$

$$s_i = \frac{h_i w_i - \min_{i=1}^n h_i w_i}{\max_{i=1}^n h_i w_i - \min_{i=1}^n h_i w_i}$$

$$IoU_i = \frac{(x'_i + w'_i - x_i)(y'_i + h'_i - y_i)}{h'_i w'_i + h_i w_i - (x'_i + w'_i - x_i)(y'_i + h'_i - y_i)} \quad (5)$$

where s_i represents the area of ground truth i after normalization, IoU_i represents the ratio of the intersection area of predicted box i and ground truth i to the area of the disease. $\ln(2 - s_i)$ is an adjustment factor that enables the network to adaptively adjust the position loss of the object based on its size.

!!!DATA!!As shown in the figure, the imbalance of regression loss is mainly reflected in larger objects receiving higher penalties compared to smaller objects. Therefore, SFL mainly suppresses this imbalance. It is not difficult to find that $\ln(2 - s_i)$ is a subtraction function with the predicted box size as the independent variable. Under the influence of this regulatory factor, the smaller the object size, the greater the increase in the proportion of object position loss. Conversely, the larger the object size, the greater the decrease in object position loss. In this way, the network will have more sufficient monitoring signals for small objects, and the training of the object detection network will be more balanced. SFL is easily integrated into any detection framework, with almost no additional burden during training and inference. The additional cost only comes from the loss statistics calculation, which can be almost negligible compared to the more computationally

intensive forward and backward propagation. β is a hyperparameter used to control the magnitude of the regulatory factor's effect on position loss.

IV. EXPERIMENTS

A. Datasets

AI-TOD: The AI-TOD dataset [10] collects 28,036 images from five publicly available and large-scale remote sensing datasets. It is specifically tailored for the challenging task of tiny object detection in aerial imagery. In AI-TOD, 700,621 object instances are meticulously annotated with an average size of just 12.8 pixels. These instances are categorized into eight distinct classes: airplane (AI), bridge (BR), storage-tank (ST), ship (SH), swimming-pool (SP), vehicle (VE), person (PE), and wind-mill (WM). Moreover, the objects are further classified based on their absolute sizes into very tiny (2 ~ 8 pixels), tiny (8 ~ 16 pixels), small (16 ~ 32 pixels), and medium (32 ~ 64 pixels) groups, with no large objects included. There are 40%(11,214), 10%(2,804), and 50%(14,018) images for training, validation, and testing.

AI-TOD-v2: It is an upgraded version of original AI-TOD dataset [10].

VisDrone2019: [51]

Hyphens and periods should not be used in equation numbers, i.e., use (1a) rather than (1-a) and (2a) rather than (2.a) for sub-equations. This should be consistent throughout the article.

DOTA-v2.0:

B. Implementation Details

All the experiments in this paper are conducted on two RTX 3080Ti GPUs with the batch size of 4.

C. Evaluation Metrics

The Microsoft COCO benchmark [52] is widely used for evaluating object detection models, owing to its fine-grained assessment of a model's ability across varying IoU thresholds. Following this standard, we employ the average precision (AP), $AP_{0.5}$, and $AP_{0.75}$ as quantitative measures to evaluate the detection performance. Furthermore, TOD focuses on tiny objects with smaller than 16×16 pixels [10], while COCO defines small objects that occupy an area less than 32×32 pixels. To accurately reflect our model's performance, we adopt AP_{vt} (very tiny), AP_t (tiny), AP_s (small), and AP_m (medium) as additional metrics.

D. Comparative Experiments

E. Generalization Experiments

It is necessary to evaluate the generalization capability of the proposed method in different aerial scenarios. Therefore, we select one

F. Ablation Studies

Experiments are performed by gradually increasing or changing the modules of the baseline to demonstrate the effectiveness of the method, so as to validate the effectiveness of the proposed method.

TABLE I
QUANTITATIVE RESULTS (I.E., PERCENTAGE OF AP SCORES) OF OUR DETECTOR WITH SOME REPRESENTATIVE DETECTORS ON AI-TOD DATASET. THE BEST RESULT IS HIGHLIGHTED IN **BOLD**. ‘NG’ INDICATES THAT THE ORIGINAL PUBLICATION DID NOT GIVE THE CORRESPONDING VALUES.

Methods	Venue	Backbone	AP	$AP_{0.5}$	$AP_{0.75}$	AP_{vt}	AP_t	AP_s	AP_m	AI	BR	ST	SH	SP	VE	PE	WM
Anchor-based Detectors:																	
RetinaNet [30]	ICCV’2017	ResNet-50	8.7	22.3	4.8	2.4	8.9	12.2	16.0	0.0	6.6	1.8	20.9	0.1	5.7	1.8	0.5
TridentNet [36]	ICCV’2019	ResNet-50	7.5	20.9	3.6	1.0	5.8	12.6	14.0	9.7	0.8	12.3	17.1	3.2	11.9	4.0	0.9
Faster R-CNN [7]	TPAMI’2017	ResNet-50	11.4	27.0	8.0	0.0	8.3	23.1	24.5	22.7	3.9	20.2	19.0	8.9	11.9	4.5	0.3
YOLOv5 [33]	ArXiv’2022	CSP-DarkNet	11.9	28.5	7.6	3.1	12.0	14.2	20.3	9.3	6.4	20.3	32.9	0.9	19.3	5.3	0.7
Cascade R-CNN [8]	CVPR’2018	ResNet-50	13.8	30.8	10.5	0.0	10.6	25.5	26.6	25.6	7.5	23.3	23.6	10.8	14.1	5.3	0.0
DoTD [48]	CVPRW’2021	ResNet-50	16.1	39.2	10.6	8.3	17.6	18.1	22.1					NG			
CFINet [53]	ICCV’2023	ResNet-50	20.1	49.1	11.3	3.8	20.7	25.9	36.6	40.0	6.8	35.5	33.5	15.7	20.9	7.9	0.6
DINO-Deformable-DETR [54]	ICLR’2023	ResNet-50	23.2	56.6	15.4	9.9	23.1	29.3	37.6					NG			
NWD-RKA [21]	ISPRS’2022	ResNet-50	23.4	53.5	16.8	8.7	23.8	28.5	36.0					NG			
RFLA [22]	ECCV’2022	ResNet-50	24.8	55.2	18.5	9.3	24.8	30.3	38.2					NG			
DNTR [55]	TGRS’2024	ResNet-50	26.2	56.7	20.2	12.8	26.4	31.0	37.0					NG			
Anchor-free Detectors:																	
FoveaBox [41]	TIP’2020	ResNet-50	8.1	19.8	5.1	0.9	5.8	13.4	15.9	13.8	0.0	18.5	17.7	0.0	11.4	3.4	0.0
RepPoints [40]	ICCV’2019	ResNet-50	9.2	23.6	5.3	2.5	9.2	12.9	14.4	2.9	2.3	21.4	26.4	0.0	15.2	5.4	0.0
CornerNet [37]	ECCV’2018	Hourglass-104	9.0	25.4	4.3	2.9	12.9	11.5	7.0	10.6	11.8	14.1	16.9	4.4	7.0	4.8	2.7
Grid R-CNN [39]	CVPR’2019	ResNet-50	12.2	27.7	9.0	0.2	10.3	22.6	23.3	22.6	8.6	18.9	22.0	7.3	12.9	4.8	0.4
CenterNet [38]	ICCV’2019	DLA-34	13.4	39.2	5.0	3.8	12.1	17.7	18.9	17.4	9.5	25.9	21.9	6.2	16.5	8.1	1.9
FCOS [42]	ICCV’2019	ResNet-50	12.6	30.4	8.1	2.3	12.2	17.2	25.0	19.3	7.4	26.1	27.4	5.8	17.4	5.6	2.6
M-CenterNet [10]	ICPR’2021	DLA-34	14.5	40.7	6.4	6.1	15.0	19.4	20.4	18.6	10.6	27.6	22.3	7.5	18.6	9.2	2.0
YOLOv8 [45]	ArXiv’2023	ResNet-50	14.9	32.5	11.6	4.5	14.4	19.0	29.3					NG			
YOLOx [44]	ArXiv’2021	CSPDarknet-53	21.1	48.6	14.7	7.7	21.4	28.9	33.9	33.8	12.2	37.1	33.6	15.9	27.3	13.5	4.2
FSANet [47]	TGRS’2022	Swin-T	22.6	52.8	15.6	7.4	21.6	29.1	38.5	30.9	15.1	35.0	40.3	19.8	24.9	8.9	5.6
Ours:																	
YOLOx w/ SA^2B -SAL	-	CSPDarknet-53	26.6	59.1	20.8	10.0	26.0	33.7	39.9	38.9	16.5	40.3	40.8	22.1	29.7	16.9	7.9
YOLOv5 w/ SA^2B -SAL	-	CSPDarknet-53	29.6	62.6	24.1	11.4	28.7	38.6	47.4	44.5	19.7	43.3	42.0	26.9	33.7	16.2	10.6

TABLE II
COMPARISON RESULTS ON VisDrone2019 AND DOTA-v2.0
VALIDATION SETS. ‘*’ DENOTES THE DETECTOR WITH SA^2B AND SFL.

Datasets	Methods	AP	AP_{50}	AP_{75}	AP_{vt}	AP_t	AP_s	AP_m
VisDrone2019	YOLOx	23.9	40.2	24.1	4.3	10.6	21.2	34.7
	YOLOx*	26.1 ^{+2.2}	43.4 ^{+3.2}	26.4 ^{+2.3}	6.2 ^{+1.9}	12.0 ^{+1.4}	22.9 ^{+1.7}	37.3 ^{+2.6}
DOTA-v2.0	YOLOx	39.5	61.3	41.4	2.1	9.4	27.2	46.8
	YOLOx*	40.1 ^{+0.6}	63.0 ^{+1.7}	42.4 ^{+1.0}	2.3 ^{+0.2}	10.7 ^{+1.3}	31.3 ^{+4.1}	46.4 ^{-0.4}

- 1) *Effectiveness of individual component:* The Values in the Table Are Recorded in Percentage.
2) *Performance of different adjust factor:*

TABLE III
AI-TOD V2

Methods	Publication	Backbone	AP	AP_{50}	AP_{75}	AP_{vt}	AP_t	AP_s	AP_m
Two-Stage Detectors:									
TridentNet [36]	ICCV'2019	ResNet-50	10.1	24.5	6.7	0.1	6.3	19.8	31.9
Faster R-CNN [7]	ArXiv'2015	ResNet-50	12.8	29.9	9.4	0.0	9.2	24.6	37.0
Cascade R-CNN [8]	CVPR'2018	ResNet-50	15.1	34.2	11.2	0.1	11.5	26.7	38.5
DetectoRS [56]	CVPR'2021	ResNet-50	16.1	35.5	12.5	0.1	12.6	28.3	40.0
DotD [48]	CVPRW'2021	ResNet-50	20.4	51.4	12.3	8.5	21.1	24.6	30.4
RFLA [22]	ECCV'2022	ResNet-50	25.7	58.9	18.8	9.2	25.5	30.2	40.2
CFINet [53]	ICCV'2023	ResNet-50							
RepPoints [40]	ICCV'2019	ResNet-50	9.3	23.6	5.4	2.8	10.0	12.3	18.9
One-Stage Detectors:									
YOLOv3 [31]	CoRR'2018	Darknet-53	4.1	14.6	0.9	1.1	4.8	7.7	8.0
RetinaNet [30]	ICCV'2017	ResNet-50	8.9	24.2	4.6	2.7	8.4	13.1	20.4
SSD-512 [29]	ECCV'2016	ResNet-50	10.7	32.5	4.0	2.0	8.7	16.8	28.0
FCOS [42]	ICCV2019	ResNet-50	12.0	30.2	7.3	2.2	11.1	16.6	26.9
YOLOx [44]	ArXiv'2021	CSPDarknet-53	23.7	55.2	16.4	9.0	22.8	29.8	40.1
Ours		CSPDarknet-53	26.3	58.2	20.4	13.7	24.3	33.5	44.8

TABLE IV
AI-TOD V2 PER CLASS

Method	Publication	Backbone	AI	BR	ST	SH	SP	VE	PE	WM
Two-Stage Detectors:										
TridentNet [36]	ICCV'2019	ResNet-50	19.3	0.1	17.2	16.2	12.4	12.5	3.4	0.0
Faster R-CNN [7]	ArXiv'2015	ResNet-50	19.7	4.8	19.0	19.9	3.7	14.4	4.8	0.0
Cascade R-CNN [8]	CVPR'2018	ResNet-50	26.2	9.6	24.0	24.3	13.2	17.5	5.8	0.1
DetectoRS [56]	CVPR'2021	ResNet-50	28.5	11.7	23.2	26.4	14.9	17.6	6.5	0.2
DotD [48]	CVPRW'2021	ResNet-50	18.7	17.5	34.7	37.0	12.4	25.4	10.3	7.4
RFLA [22]	ECCV'2022	ResNet-50								
CFINet [53]	ICCV'2023	ResNet-50								
RepPoints [40]	ICCV'2019	ResNet-50	0.0	0.1	22.5	28.8	0.2	18.3	4.1	0.0
One-Stage Detectors:										
YOLOv3 [31]	CoRR'2018	Darknet-53	0.3	0.5	8.5	9.4	0.0	12.7	1.4	0.0
RetinaNet [30]	ICCV'2017	ResNet-50	1.3	11.8	14.3	23.6	5.8	11.4	2.3	0.5
SSD-512 [29]	ECCV'2016	ResNet-50	14.9	9.6	13.2	18.2	10.6	12.7	2.9	3.1
FCOS [42]	ICCV2019	ResNet-50	7.2	13.4	20.2	26.7	8.4	16.3	3.5	0.0
YOLOx [44]	ArXiv'2021	CSPDarknet-53	36.2	13.6	38.1	36.1	15.0	28.8	15.2	6.4
Ours		CSPDarknet-53	41.7	17.0	38.8	38.4	20.0	29.8	16.8	7.8

TABLE V
ABLATION STUDY OF INDIVIDUAL EFFECTIVENESS OF SA^2B AND SFL ON AI-TOD DATASET. THE VALUES IN THE TABLE ARE RECORDED IN PERCENTAGE.

YOLOx	SA^2B	SFL	AP	AP_{50}	AP_{75}	AP_{vt}	AP_t	AP_s	AP_m	AI	BR	ST	SH	SP	VE	PE	WM
✓			22.2	52.4	15.2	7.7	21.2	29.7	35.5	33.8	12.2	37.1	33.6	15.9	27.3	13.5	4.2
✓	✓		24.0	55.4	17.7	9.1	23.6	30.5	37.1	37.2	14.3	39.2	36.2	18.0	28.1	15.3	3.7
✓		✓	23.7	55.3	17.1	8.5	22.8	29.9	37.6	37.0	13.7	37.6	35.8	16.7	28.7	14.7	5.4
✓	✓	✓	26.6	59.1	20.8	10.0	26.0	33.7	39.9	38.9	16.5	40.3	40.8	22.1	29.7	16.9	7.9

TABLE VI
ABLATION RESULTS (I.E., PERCENTAGE OF AP SCORES) OF INDIVIDUAL EFFECTIVENESS OF SA^2B AND SFL ON AI-TOD DATASET.

YOLOv5	SA^2B	SFL	AP	AP_{50}	AP_{75}	AP_{vt}	AP_t	AP_s	AP_m	AI	BR	ST	SH	SP	VE	PE	WM
✓			11.9	28.5	7.6	3.1	12.0	14.2	20.3	9.3	6.4	20.3	32.9	0.9	19.3	5.3	0.7
✓	✓		27.4	61.5	20.5	9.4	26.5	35.6	44.7	42.6	17.8	41.4	38.0	23.8	31.7	14.7	9.6
✓		✓	28.8	62.2	22.9	9.5	28.0	37.4	48.2	44.6	19.9	42.5	40.4	26.3	32.4	16.1	8.4
✓	✓	✓	29.6	62.6	24.1	11.4	28.7	38.6	47.4	44.5	19.7	43.3	42.0	26.9	33.7	16.2	10.6

TABLE VII
ABLATION RESULTS (I.E., PERCENTAGE OF AP SCORES) OF THE DIFFERENT FACTOR β IN THE SFL ON AI-TOD DATASET.

β	AP	AP_{50}	AP_{75}	AP_{vt}	AP_t	AP_s	AP_m	AI	BR	ST	SH	SP	VE	PE	WM
1	24.6	56.6	17.7	9.0	23.5	31.3	38.2	37.9	14.2	39.3	36.6	18.7	28.4	15.9	5.5
1/ln 2	25.0	56.2	18.8	9.6	23.6	38.0	38.7	37.6	15.4	39.4	38.4	18.7	28.9	16.2	5.0
2/ln 2	26.6	59.1	20.8	10.0	26.0	33.7	39.9	38.9	16.5	40.3	40.8	22.1	29.7	16.9	7.9

V. CONCLUSION

In this paper,

REFERENCES

- [1] L. P. Osco, M. dos Santos de Arruda, D. N. Gonçalves, A. Dias, J. Batistoti, M. de Souza, F. D. G. Gomes, A. P. M. Ramos, L. A. de Castro Jorge, V. Liesenberg, J. Li, L. Ma, J. Marcato, and W. N. Gonçalves, "A cnn approach to simultaneously count plants and detect plantation-rows from uav imagery," *ISPRS Journal of Photogrammetry and Remote Sensing*, vol. 174, pp. 1–17, 2021.
- [2] Q. Ge, W. Da, and M. Wang, "Marfpnet: Multiattention and adaptive reparameterized feature pyramid network for small target detection on water surfaces," *IEEE Transactions on Instrumentation and Measurement*, vol. 73, pp. 1–17, 2024.
- [3] M. Ren, X. Zhang, X. Chen, B. Zhou, and Z. Feng, "Yolov5s-m: A deep learning network model for road pavement damage detection from urban street-view imagery," *International Journal of Applied Earth Observation and Geoinformation*, vol. 120, JUN 2023.
- [4] Z. Zheng, Y. Zhong, J. Wang, A. Ma, and L. Zhang, "Building damage assessment for rapid disaster response with a deep object-based semantic change detection framework: From natural disasters to man-made disasters," *Remote Sensing of Environment*, vol. 265, p. 112636, 2021.
- [5] K. Tong and Y. Wu, "Deep learning-based detection from the perspective of small or tiny objects: A survey," *Image and Vision Computing*, vol. 123, JUL 2022.
- [6] X. Zhang, T. Zhang, G. Wang, P. Zhu, X. Tang, X. Jia, and L. Jiao, "Remote sensing object detection meets deep learning: A metareview of challenges and advances," *IEEE Geoscience and Remote Sensing Magazine*, OCT 2023.
- [7] S. Ren, K. He, R. Girshick, and J. Sun, "Faster r-cnn: Towards real-time object detection with region proposal networks," *IEEE Transactions on Pattern Analysis and Machine Intelligence*, vol. 39, no. 6, pp. 1137–1149, 2017.
- [8] Z. Cai and N. Vasconcelos, "Cascade r-cnn: Delving into high quality object detection," in *2018 IEEE/CVF Conference on Computer Vision and Pattern Recognition*, 2018, pp. 6154–6162.
- [9] N. Carion, F. Massa, G. Synnaeve, N. Usunier, A. Kirillov, and S. Zagoruyko, "End-to-end object detection with transformers," in *Computer Vision – ECCV 2020*, A. Vedaldi, H. Bischof, T. Brox, and J.-M. Frahm, Eds. Cham: Springer International Publishing, 2020, pp. 213–229.
- [10] J. Wang, W. Yang, H. Guo, R. Zhang, and G.-S. Xia, "Tiny object detection in aerial images," in *2020 25th International Conference on Pattern Recognition (ICPR)*, 2021, pp. 3791–3798.
- [11] B. Bosquet, D. Cores, L. Seidenari, V. M. Brea, M. Mucientes, and A. Del Bimbo, "A full data augmentation pipeline for small object detection based on generative adversarial networks," *Pattern Recognition*, vol. 133, p. 108998, 2023.
- [12] P. Shamsolmoali, M. Zareapoor, J. Chanussot, H. Zhou, and J. Yang, "Rotation equivariant feature image pyramid network for object detection in optical remote sensing imagery," *IEEE Transactions on Geoscience and Remote Sensing*, vol. 60, pp. 1–14, 2021.
- [13] B. Zhao, Y. Wu, X. Guan, L. Gao, and B. Zhang, "An improved aggregated-mosaic method for the sparse object detection of remote sensing imagery," *Remote Sensing*, vol. 13, no. 13, 2021.
- [14] J. Xiao, H. Guo, J. Zhou, T. Zhao, Q. Yu, Y. Chen, and Z. Wang, "Tiny object detection with context enhancement and feature purification," *Expert Systems with Applications*, vol. 211, p. 118665, 2023.
- [15] K. Cheng, H. Cui, H. A. Ghafoor, H. Wan, Q. Mao, and Y. Zhan, "Tiny object detection via regional cross self-attention network," *IEEE Transactions on Circuits and Systems for Video Technology*, 2022.
- [16] J. Chen, H. Hong, B. Song, J. Guo, C. Chen, and J. Xu, "Mdct: Multi-kernel dilated convolution and transformer for one-stage object detection of remote sensing images," *Remote Sensing*, vol. 15, no. 2, p. 371, 2023.
- [17] M. Hong, S. Li, Y. Yang, F. Zhu, Q. Zhao, and L. Lu, "Sspnet: Scale selection pyramid network for tiny person detection from uav images," *IEEE geoscience and remote sensing letters*, vol. 19, pp. 1–5, 2021.
- [18] Y. Li, Q. Huang, X. Pei, Y. Chen, L. Jiao, and R. Shang, "Cross-layer attention network for small object detection in remote sensing imagery," *IEEE Journal of Selected Topics in Applied Earth Observations and Remote Sensing*, vol. 14, pp. 2148–2161, 2021.
- [19] W. Huang, G. Li, B. Jin, Q. Chen, J. Yin, and L. Huang, "Scenario context-aware-based bidirectional feature pyramid network for remote sensing target detection," *IEEE Geoscience and Remote Sensing Letters*, vol. 19, 2022.
- [20] R. Dong, D. Xu, J. Zhao, L. Jiao, and J. An, "Sig-nms-based faster r-cnn combining transfer learning for small target detection in vhr optical remote sensing imagery," *IEEE Transactions on Geoscience and Remote Sensing*, vol. 57, no. 11, pp. 8534–8545, NOV 2019.
- [21] C. Xu, J. Wang, W. Yang, H. Yu, L. Yu, and G.-S. Xia, "Detecting tiny objects in aerial images: A normalized wasserstein distance and a new benchmark," *ISPRS Journal of Photogrammetry and Remote Sensing*, vol. 190, pp. 79–93, 2022.
- [22] Xu, Chang and Wang, Jinwang and Yang, Wen and Yu, Huai and Yu, Lei and Xia, Gui-Song, "Rfla: Gaussian receptive field based label assignment for tiny object detection," in *17th European Conference on Computer Vision (ECCV)*, vol. 13669, 2022, pp. 526–543.
- [23] H. Zhang, C. Xu, and S. Zhang, "Inner-iou: More effective intersection over union loss with auxiliary bounding box," 2023. [Online]. Available: <https://arxiv.org/abs/2311.02877>
- [24] T.-Y. Lin, P. Dollár, R. Girshick, K. He, B. Hariharan, and S. Belongie, "Feature pyramid networks for object detection," in *Proceedings of the*

- IEEE Conference on Computer Vision and Pattern Recognition (CVPR)*, 2017, pp. 2117–2125.
- [25] S. Liu, L. Qi, H. Qin, J. Shi, and J. Jia, “Path aggregation network for instance segmentation,” in *Proceedings of the IEEE Conference on Computer Vision and Pattern Recognition (CVPR)*, 2018, pp. 8759–8768.
 - [26] M. Tan, R. Pang, and Q. Le, V, “Efficientdet: Scalable and efficient object detection,” in *IEEE/CVF Conference on Computer Vision and Pattern Recognition (CVPR)*, 2020, pp. 10 778–10 787.
 - [27] H. Rezatofighi, N. Tsoi, J. Gwak, A. Sadeghian, I. Reid, and S. Savarese, “Generalized intersection over union: A metric and a loss for bounding box regression,” in *IEEE/CVF Conference on Computer Vision and Pattern Recognition (CVPR)*, 2019, pp. 658–666.
 - [28] Z. Zheng, P. Wang, W. Liu, J. Li, R. Ye, and D. Ren, “Distance-iou loss: Faster and better learning for bounding box regression,” in *National Conference on Artificial Intelligence (AAAI)*, vol. 34, 2020, pp. 12 993–13 000.
 - [29] W. Liu, D. Anguelov, D. Erhan, C. Szegedy, S. Reed, C.-Y. Fu, and A. C. Berg, “Ssd: Single shot multibox detector,” in *14th European Conference on Computer Vision (ECCV)*, vol. 9905, 2016, pp. 21–37.
 - [30] T.-Y. Lin, P. Goyal, R. Girshick, K. He, and P. Dollár, “Focal loss for dense object detection,” in *Proceedings of the IEEE international conference on computer vision (ICCV)*, 2017, pp. 2980–2988.
 - [31] J. Redmon, “Yolov3: An incremental improvement,” *arXiv preprint arXiv:1804.02767*, 2018.
 - [32] A. Bochkovskiy, C.-Y. Wang, and H.-Y. M. Liao, “Yolov4: Optimal speed and accuracy of object detection,” *ArXiv*, vol. abs/2004.10934, 2020.
 - [33] Ultralytics, “ultralytics/yolov5: v6.0 - yolov5n ‘nano’ models, roboflow integration, tensorflow export, opencv dnn support,” feb 2021. [Online]. Available: <https://doi.org/10.5281/zenodo.5563715>
 - [34] R. Girshick, J. Donahue, T. Darrell, and J. Malik, “Rich feature hierarchies for accurate object detection and semantic segmentation,” in *IEEE Conference on Computer Vision and Pattern Recognition (CVPR)*, 2014, pp. 580–587.
 - [35] R. Girshick, “Fast R-CNN,” in *IEEE International Conference on Computer Vision (ICCV)*, 2015, pp. 1440–1448.
 - [36] Y. Li, Y. Chen, N. Wang, and Z.-X. Zhang, “Scale-aware trident networks for object detection,” in *Proceedings of the IEEE/CVF International Conference on Computer Vision (ICCV)*, 2019, pp. 6053–6062.
 - [37] H. Law and J. Deng, “Cornernet: Detecting objects as paired keypoints,” in *15th European Conference on Computer Vision (ECCV)*, vol. 11218, 2018, pp. 765–781.
 - [38] K. Duan, S. Bai, L. Xie, H. Qi, Q. Huang, and Q. Tian, “Centernet: Keypoint triplets for object detection,” in *IEEE/CVF International Conference on Computer Vision (ICCV)*, 2019, pp. 6568–6577.
 - [39] X. Lu, B. Li, Y. Yue, Q. Li, and J. Yan, “Grid r-cnn,” in *2019 IEEE/CVF Conference on Computer Vision and Pattern Recognition (CVPR)*, 2019, pp. 7355–7364.
 - [40] Z. Yang, S. Liu, H. Hu, L. Wang, and S. Lin, “Reppoints: Point set representation for object detection,” in *Proceedings of the IEEE/CVF International Conference on Computer Vision (ICCV)*, 2019, pp. 9656–9665.
 - [41] T. Kong, F. Sun, H. Liu, Y. Jiang, L. Li, and J. Shi, “Foveabox: Beyond anchor-based object detection,” *IEEE Transactions on Image Processing*, vol. 29, pp. 7389–7398, 2020.
 - [42] Z. Tian, C. Shen, H. Chen, and T. He, “FCOS: a simple and strong anchor-free object detector,” *IEEE Transactions on Pattern Analysis and Machine Intelligence*, vol. 44, no. 4, pp. 1922–1933, 2020.
 - [43] C. Feng, Y. Zhong, Y. Gao, M. R. Scott, and W. Huang, “Tood: Task-aligned one-stage object detection,” in *2021 IEEE/CVF International Conference on Computer Vision (ICCV)*. IEEE Computer Society, 2021, pp. 3490–3499.
 - [44] Z. Ge, S. Liu, F. Wang, Z. Li, and J. Sun, “Yolox: Exceeding yolo series in 2021,” *ArXiv*, vol. abs/2107.08430, 2021.
 - [45] G. Jocher, A. Chaurasia, and J. Qiu, Ultralytics yolo. 2023, Jan. [Online]. Available: <https://github.com/ultralytics/ultralytics>
 - [46] V. Chalavadi, P. Jeripothula, R. Datla, S. B. Ch et al., “msodanet: A network for multi-scale object detection in aerial images using hierarchical dilated convolutions,” *Pattern Recognition*, vol. 126, p. 108548, 2022.
 - [47] J. Wu, Z. Pan, B. Lei, and Y. Hu, “FSANet: feature-and-spatial-aligned network for tiny object detection in remote sensing images,” *IEEE Transactions on Geoscience and Remote Sensing*, vol. 60, 2022.
 - [48] C. Xu, J. Wang, W. Yang, and L. Yu, “Dot distance for tiny object detection in aerial images,” in *Proceedings of the IEEE/CVF conference on computer vision and pattern recognition (CVPR)*, 2021, pp. 1192–1201.
 - [49] Z. Zhou and Y. Zhu, “Kldet: Detecting tiny objects in remote sensing images via kullback-leibler divergence,” *IEEE Transactions on Geoscience and Remote Sensing*, vol. 62, pp. 1–16, 2024.
 - [50] N. Su, Z. Zhao, Y. Yan, J. Wang, W. Lu, H. Cui, Y. Qu, S. Feng, and C. Zhao, “Mmpw-net: Detection of tiny objects in aerial imagery using mixed minimum point-wasserstein distance,” *Remote Sensing*, vol. 16, no. 23, 2024. [Online]. Available: <https://www.mdpi.com/2072-4292/16/23/4485>
 - [51] P. Zhu, L. Wen, D. Du, X. Bian, H. Fan, Q. Hu, and H. Ling, “Detection and tracking meet drones challenge,” *IEEE Transactions on Pattern Analysis and Machine Intelligence*, vol. 44, no. 11, pp. 7380–7399, 2021.
 - [52] T.-Y. Lin, M. Maire, S. Belongie, J. Hays, P. Perona, D. Ramanan, P. Dollár, and C. L. Zitnick, “Microsoft coco: Common objects in context,” in *Proceedings of the 13th European Conference on Computer Vision (ECCV)*, aug 2014, pp. 740–755.
 - [53] X. Yuan, G. Cheng, K. Yan, Q. Zeng, and J. Han, “Small object detection via coarse-to-fine proposal generation and imitation learning,” in *Proceedings of the IEEE/CVF international conference on computer vision*, 2023, pp. 6317–6327.
 - [54] H. Zhang, F. Li, S. Liu, L. Zhang, H. Su, J. Zhu, L. M. Ni, and H.-Y. Shum, “Dino: Detr with improved denoising anchor boxes for end-to-end object detection,” in *Proceedings of the IEEE/CVF Conference on Computer Vision and Pattern Recognition (ICLR)*, 2023.
 - [55] H.-I. Liu, Y.-W. Tseng, K.-C. Chang, P.-J. Wang, H.-H. Shuai, and W.-H. Cheng, “A denoising fpn with transformer r-cnn for tiny object detection,” *IEEE Transactions on Geoscience and Remote Sensing*, vol. 62, pp. 1–15, 2024.
 - [56] S. Qiao, L.-C. Chen, and A. Yuille, “Detectors: Detecting objects with recursive feature pyramid and switchable atrous convolution,” in *Proceedings of the IEEE/CVF conference on computer vision and pattern recognition (CVPR)*, 2021, pp. 10 213–10 224.